TALIF measurements of hydrogen and deuterium surface loss probabilities on quartz in low pressure high density plasmas

X Yang, D Kogut, L Couëdel, T Angot, P Roubin, J.-B Faure, Gilles Cartry

TALIF measurements of hydrogen and deuterium surface loss probabilities on quartz in low pressure high density plasmas

X. Yang,[1,2,*] D. Kogut,[1] L. Couëdel,[1,3] T. Angot,[1]
P. Roubin,[1] J.-B. Faure,[1] and G. Cartry[1,†]

[1]*Aix-Marseille Université, CNRS, PIIM,*
UMR 7345, Centre Scientifique de Saint Jérôme,
case 241, 13397 Marseille Cedex 20, France
[2]*Institute of Plasma Physics, CAS,*
Shushanhu road 350, Hefei, Anhui, 230031, China
[3]*Department of Physics and Engineering Physics,*
University of Saskatchewan, Saskatoon, SK S7N 5E2, Canada

(Dated: December 29, 2020)

Abstract

This article deals with surface loss on quartz of atomic hydrogen (H) and its isotope deuterium (D) in a low-pressure (10 Pa) pulsed inductively coupled plasma. The atomic temporal decay in the post discharge is measured by Two-photon Absorption Laser-Induced Fluorescence (TALIF). From the loss rate, the atomic surface loss probability is determined. In pure hydrogen or pure deuterium gas, no isotopic effect on surface kinetics has been observed and the surface loss probabilities of H and D were found to be almost identical and equal to ∼1.8%. However, despite the lack of difference in surface loss probability, a net isotopic effect on surface loss rate due to the mass difference between the isotopes is measured. Hydrogen atoms diffuse faster and have higher flux to the plasma chamber walls than deuterium atoms. Hydrogen atoms are therefore lost at higher rate than deuterium atoms. Based on the observed isotopic difference and on the comparison between H and D TALIF signals, the isotopic effects on H and D atom production are discussed.

PACS numbers: 52.40.Hf

I. INTRODUCTION

In low-pressure plasma sources, due to low collisionality and fast diffusion, the surface chemistry on the reactor walls in contact with the plasma plays a major role on the plasma equilibrium [1]. Radical densities depend on chemical reactions at the wall rather than reactions in the plasma volume. This surface chemistry leads to complexity in industrial plasma processes, such as those employed in the microelectronics industry, because surface state must be controlled perfectly to obtain reproducible results. This issue is usually fixed by employing systematic wall conditioning procedure before any process [1]. Nevertheless, the radical densities in the plasma are set by wall reactions, the rate coefficients of which are poorly known, preventing efficient development support from plasma modelling. Even in simple chemistry, when using gases such as oxygen, hydrogen, nitrogen, surface chemistry is a key issue as it determines directly the concentration of the active atomic species. The loss of atomic species at the wall, whether through sticking or recombination into molecules, is hard to predict theoretically because it strongly depends on the surface state which in turn

* xin.yang@ipp.ac.cn

† gilles.cartry@univ-amu.fr

is depending on the plasma conditions through the ion flux towards the wall, the energy of ions impinging the wall, the atomic flux, etc. As a consequence, the surface loss probability, which is the probability for an atomic species to be lost by any mechanism when hitting the wall, is often used as a fitting parameter in models. The best solution, when possible, is to measure it in-situ, in the plasma source of interest. The goal of this article is to determine the hydrogen and deuterium atomic loss on plasma quartz walls in a low pressure high density inductively coupled plasma source.

Hydrogen atom (H) surface losses in low-pressure plasma is of interest for many applications such as plasma etching in microelectronics, surface cleaning, etc. Deuterium atom (D) surface losses in low-pressure plasma are of interest in the context of magnetically confined fusion plasmas. In tokamaks (magnetic confinement fusion reactors) surface reactions of hydrogen/deuterium atoms at reactor walls affect the fuelling efficiency, the plasma density control and the density of neutral hydrogen at the plasma boundary, which impacts particle and energy transport [2]. Atomic surface reactions in tokamaks refer to retention (sticking on the surface or introduction of hydrogen inside the wall volume) and recycling (formation of molecules at the wall). Recycling of hydrogen atoms forming molecules directly impacts the plasma edge composition and is of primary importance in the so-called detached plasma regime [3] which is targeted for ITER operation [4]. The ultimate goal of our research program is to measure atomic losses at the surface of fusion relevant materials (tungsten as a priority, but also tungsten nitrides, stainless steel, etc). To this end, a low pressure plasma source has been specially developed [5]. It consists of an inductively coupled plasma confined by quartz walls interacting with a sample made of the material of interest, and equipped with Two photon Absorption Laser Induced Fluorescence (TALIF) diagnostics. TALIF measurements give access to surface loss probabilities. As surface loss probabilities depend on plasma conditions and may vary from one source to another, the objective is mostly to give trends such as variations induced by the type of material, surface temperature, ion flux, etc. As a first step, atomic losses on quartz need to be determined since quartz is the main wall material of our plasma source. In the present article, H and D atomic loss probabilities on quartz are determined using time resolved TALIF measurements in pulsed (10 Hz) hydrogen/deuterium plasmas. In the plasma post-discharge, no molecular dissociation occurs anymore and the atomic decays measured by TALIF are directly related to surface loss.

The first part of the article presents the experimental set-up and describes the TALIF diagnostic system. Details on TALIF calibration are given. In the second part, time resolved TALIF measurements in pure H_2, pure D_2 and in $H_2 : D_2$ mixtures are presented. Surface loss probabilities are then calculated. Finally, the results are discussed.

II. EXPERIMENTAL SET-UP

A. Plasma chamber

The plasma reactor (see Figure 1) is composed of a stainless steel spherical plasma chamber (30 cm in diameter) with a top quartz window (166 mm in diameter, 12 mm thick) allowing for RF power coupling between an external three turns planar coil antenna and the plasma. A temperature controlled sample holder of 145 mm diameter is placed opposite the quartz window at a distance of 149 mm. It is associated to a load-lock system for fast introduction under vacuum of 10 cm sample wafers. This sample holder is designed to study atomic surface loss probabilities on various materials. However, in the present study, a quartz disc (172 mm diameter and 3 mm thickness) has been installed on top of the sample holder and fully covers it. The plasma region is radially limited by a cylindrical quartz tube (160 mm internal diameter, 5 mm thickness and 140 mm height) placed between the bottom quartz disc and the top quartz window. The plasma is therefore almost completely surrounded by quartz walls. Only a 5 mm height gap remains between the lateral quartz tube and the quartz top window to allow for gas pumping, as well as a small 1 mm gap between the cylinder tube and the bottom quartz disc.

The plasma chamber is equipped with one ionisation gauge (54132-GE02 Granville Phillips) to measure the base pressure ($\sim 2 \cdot 10^{-6}$ Pa) and MKS 121A capacitance Baratron gauge to monitor the pressure during plasma operation. Both of them are attached on the flanges of stainless steel chamber containing the quartz tube. The vacuum is ensured by Varian Turbo-V551 turbo molecular vacuum pump and an Alcatel oil rotary pump. Ultra-high purity gases (UHP 99.99) are introduced into the vacuum vessel through Brooks mass flow controllers 5850TR series from a top side window. Krypton, used for TALIF calibration, was introduced using a mini gas cylinder. During plasma operation, the pressure was regulated by an adjustable gate valve placed between the turbo molecular pump and the plasma

chamber. The total gas flow was set at 20 sccm, both for pure gas or gas mixture operation. Under these conditions, gas residence time in the plasma chamber, without considering the presence of the quartz tube, is estimated to be of the order of 10 seconds.

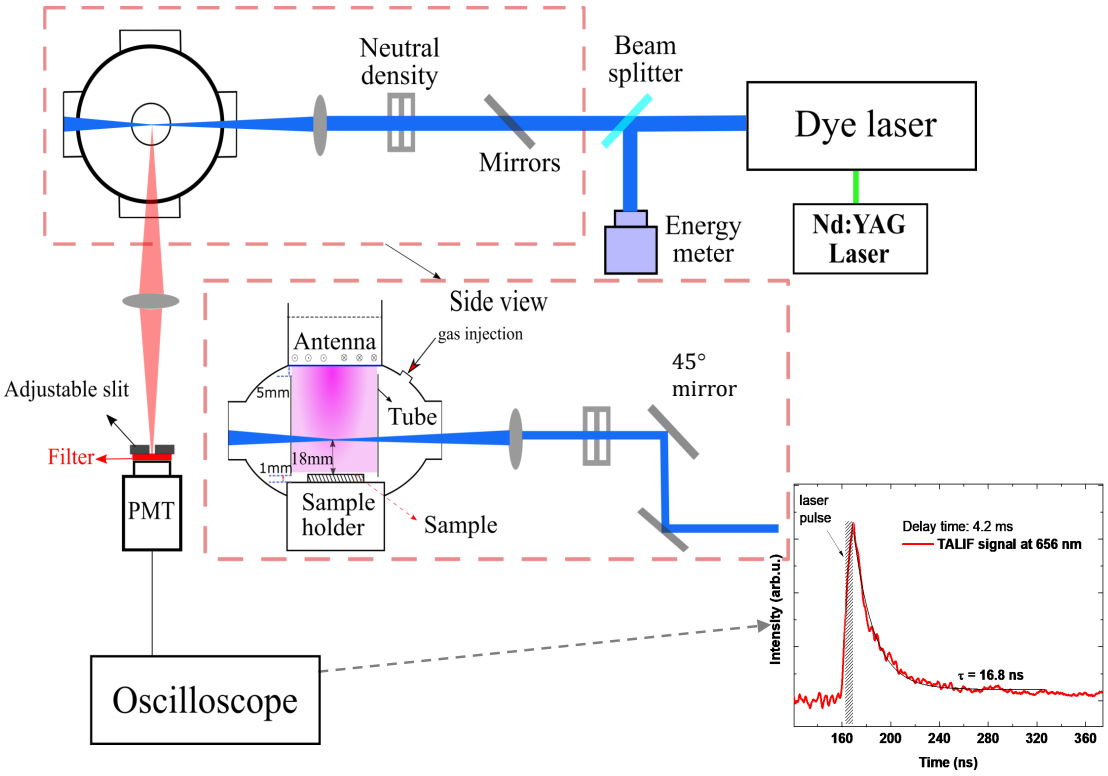

FIG. 1. Schematic of the experimental set-up. The inset shows an example of the evolution of the TALIF signal as a function of time

Pulsed Inductively coupled plasma (ICP) was used in this work to investigate plasma-surface interaction. Inductive coupling was obtained thanks to a three turns planar coil antenna placed on top of the quartz window. It is made of copper tube (6 mm diameter) cooled by internal water circulation. The outside termination of the antenna was connected to ground through a variable capacitor used to decrease the voltage at the antenna termination and to limit capacitive coupling [6]. Using high voltage probes, its value was set to ensure a virtual ground on antenna's location. The inner termination of the antenna was connected to a CesarTM 1310 Radio Frequency generator through a L-type matching box containing two variable capacitors. The two capacitors were adjusted to ensure impedance matching under different discharge conditions. The RF match box was first manually tuned to minimise the reflected power with steady plasmas. Then, with pulsed plasmas, the match-

ing was improved by fine tuning of the capacitances based on real time monitoring of the electron desnity n_e by a microwave interferometer. A Ka-band Microwave Interferometer (MWI 2650-A) was used. The operating frequency of our microwave interferometer is 26.5 GHz and its measurement range is from $\sim 10^{16} - 10^{17}$ m^{-3}. The microwave line of sight was passing through the inner quartz tube just above the sample (quartz disc at bottom), and two opposite 38 mm diameter view ports.

The working pressure was set to 10 Pa as plasma re-ignition in pulsed mode is harder at lower pressure. The input power was set to 1000 W which was the maximum available power. Lower power led to difficulties for plasma re-ignition in pulsed mode. Pulse frequency was chosen equal to 10 Hz and the duty cycle was set to a low value(10%). Discharge time t_{on} was 10 ms and post-discharge time t_{off} was 90 ms. Previous characterisation of the plasma source shows that 10 ms are long enough to reach a steady-state plasma without increasing noticeably the average wall temperature at a 10% duty cycle. Wall and sample temperatures after 40 min of pulsed plasma operation were $\sim$40°C as measured by a thermocouple. Finally, a 30 min long continuous wave (CW) plasma under capacitive mode with input power of 200 W was applied for wall conditioning purpose before each series of TALIF measurements. A Pyrex tube with a hole was used to introduce at the centre of the plasma a RF compensated Scientific System Langmuir probe 5 cm above the bottom quartz disc. Electron density and electron temperature measured at the end of the pulse are respectively $n_e = 9 \cdot 10^{16}$ m^{-3} and $T_e = 0.7$ eV giving an estimated positive ion flux onto the surfaces of $\sim 10^{20}$ m^{-2}s^{-1}.

B. TALIF measurements

Atomic H and D measurements were carried out by TALIF. Atomic H in its ground state ($1s\ ^2S_{1/2}$) was excited by simultaneous absorption of two laser photons, with a wavelength of 205 nm (205.1445 nm for H atoms and 205.0876 nm for D atoms), to the excited electronic levels $3s\ ^2S_{1/2}$ and $3d\ ^2D_j$. Excited states relaxed by spontaneous emission of a Balmer-α photon at 656.3 nm from the $3d\ ^2D_j$ and $3s\ ^2S_{1/2}$ state to the $2p\ ^2P_j$ state. Since the two-photon absorption cross section for 1s→3d transition is 7.56 times higher than for 1s→3s transition [7], the 3d→2p transition dominated the de-excitation. The fluorescence decay time which is related to the lifetime of the excited state for $3d\ ^2D_j$ is 15.5 ns [7]. Krypton gas is often employed for absolute calibration of H density measured by TALIF [8] due to its

similar two-photon absorption scheme. It has been used here for calibration and comparison purposes. Krypton (Kr) in the ground state $4p^6\ {}^1S_0$ was excited to $5p'[3/2]_2$ excited state by two photon absorption at 204.2 nm. The fluorescence to the $5s'[1/2]_1$ state was observed at 826 nm. The natural lifetime for the excited state of krypton ($5p'[3/2]_2$) is 35 ns [9].

The second harmonic wavelength (532 nm) of a Continuum's Surelite III Nd:YAG laser ($\sim$6 ns pulse, 10 Hz) pumped a NarrowScan dye laser whose output delivered wavelength at 615 nm in a $\sim$10 ns pulse. The required 205 nm wavelength was generated by frequency doubling and frequency mixing with nonlinear crystals, with an output laser energy of about 1 mJ/pulse.

Figure 1 shows a schematic of TALIF experimental system. The laser beam was guided to the plasma chamber through two parallel mirrors (25.0 mm 193 nm 45°, excimer Laser Line Mirror, Go Edmund) with a 45° angle of incidence. A series of neutral density filter mounted on a manual filter wheel station was positioned on the way of the laser beam to adjust the laser energy entering the plasma chamber. Then the laser beam was focused by an $f = 30$ cm plano-convex suprasil spherical lens at the centre of the plasma chamber and injected into the plasma chamber through a fused-silica optical access window. In order to decrease the laser beam reflection and diffusion on the quartz tube and increase the laser intensity to the measurement position, a 5 mm diameter hole was drilled on the pathway of the laser beam on one side of the tube. The laser beam passes through the chamber parallel to the surface of the quartz bottom disc at a distance of 25 mm above it. The fluorescence detection was performed perpendicularly to the laser beam through the quartz tube and a common view port. The spectral selection was achieved by an interference filter centred at 655 nm for atomic H with 40 nm bandwidth (Semrock, FF01-655/40) or centred at 842 nm for Kr with 56 nm bandpass (Semrock, FF01-842/56). An adjustable slit was placed in front of the filter to control the light flux. The slit was oriented perpendicular to the laser beam. The fluorescence photons passing through the slit were detected by a side-on Hamamatsu 9110 photomultiplier tube (PMT). A gated operation of PMT was required since the strong emission signal of the background plasma pulse was saturating the PMT and was preventing any measurement in the early post discharge. A "normally off" Hamamatsu C1392-56 gated socket assembly was used with a gate duration of 10 μs. The PMT output was recorded with an oscilloscope (LeCroy WaveSurfer 64MXs-B) through a 50 Ω input impedance for current-to-voltage conversion and was then sent to a computer for data processing. The

laser energy for each individual pulses was monitored by a power & energy meter (SOLO 2, Gentec-EO, Canada) and recorded directly on a computer thanks to a data acquisition board.

A waveform generator delivering TTL signals at 10 Hz was used as master clock to synchronise the laser shot, the plasma pulse, the gated PMT signal, the laser energy measurement, and the TALIF signal acquisition, using several delay generators. Despite the fact that plasma pulse ignition was ensured at 10 Pa, plasma pulse reproducibility was not perfect and could impact the quality of TALIF measurement in the early afterglow. The issue was solved by monitoring in real time electron density during the plasma pulse with the microwave interferometer. According to some thresholds in pulse duration and electron density values, the pulse was qualified or not for TALIF measurement. In the same way, the RF forward power related signal given by the RF generator was also used as a third condition for pulse qualification. A homemade electronic circuit was generating a TTL signal triggering the scope acquisition when all qualification requirements were met. This scheme enabled to collect a subset of pulses with good reproducibility to make reliable TALIF measurements. It is presented in details in Ref. [10].

The absorption line profiles were scanned and the relative densities of atomic hydrogen and deuterium in the post-discharge were evaluated by calculating the area under the curve. In order to ensure constant laser energy during scans, lookup tables of laser energy versus laser wavelength were previously established and used during the measurements.

Qualified TALIF signals were recorded with the oscilloscope working under 'sequence' mode. Under this mode, the TALIF signal was recorded pulse-by-pulse by the scope and stored in the internal memory. Typically, a sequence was made of 20 wavelengths and 50 trigger events for every wavelength. The output file contains 1000 fluorescence signals for one delay time acquired in a reasonable time of about 5 to 10 minutes. For data processing, the averaged TALIF signal at a given wavelength was normalised by the square of the corresponding averaged laser energy. The normalisation was performed automatically by a homemade routine.

1. *Transition saturation*

Compared to single-photon LIF, TALIF presents a quadratic dependence of the signal to the laser energy. At low laser energy, the TALIF signal is proportional to the ground-state atom density and the square of the laser energy. On the contrary at high laser energy, additional depopulation pathways of n = 3 level, such as multi-photon ionisation by a third photon absorbed [11] and two-photon-excited stimulated emission (TALISE) [12], start to compete with the radiative depopulation. To ensure that these depopulation pathways did not affect the results, the incident laser energy was varied using neutral filters and TALIF signals were recorded at constant atom density. Figure 2 shows typical results for Kr and H. For Kr measurements, the plasma chamber was filled at a pressure of 10 Pa. For atomic H and D, measurements were performed in the post-discharge plasma with two delay times of 0.05 ms and 4 ms, which respectively represented high and low atomic density. TALIF signal as a function of laser energy is plotted in Figure 2. The exponents s of the polynomial parts are between 1.74 and 1.99 for all measurements, close to the expected value of 2 for a quadratic dependence of the TALIF signal with respect to the laser energy. The saturation threshold for krypton was around 30-40 μJ. The TALIF signal of H and D atom remained in the non-saturated regime over the entire scanned range of laser energy (up to 370 μJ routinely obtained, somewhat lower than the maximum output of the dye laser 1 mJ due to losses in the beam splitter and optics and possibly to non optimised dye laser tuning). Measurements were then performed with a 370 μJ laser energy for H and D.

2. *Photomultiplier saturation*

For reliable measurements, the PMT must be used in its linear regime where the relationship between the incident light level and the anode output current is linear. Space charge limitation of the anode current was observed even at moderate TALIF signal intensity due to the high employed gain of the PMT. In order to maintain linearity over a broader range of TALIF signal intensity, a so-called 'tapered voltage-divider' circuit was inserted in the measurement circuit. The electric field between the last dynode and the anode of the PMT was increased by doubling the resistance of the biasing circuit, thus doubling the voltage drop of this last dynode stage. More details can be found in Yang's thesis [10]. In the

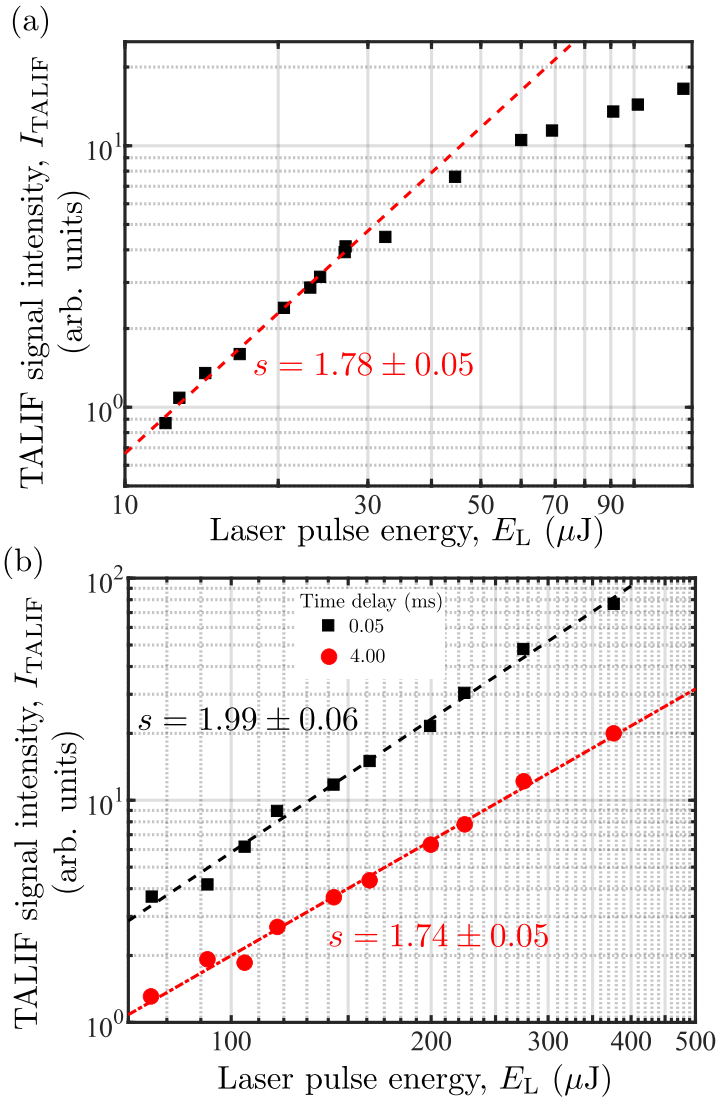

FIG. 2. TALIF signal intensity I_{TALIF} as a function of laser pulse energy E_{L}: (a) Kr at 10 Pa, and (b) hydrogen in H_2 plasma, 10 Pa, 1000 W, for two time delays in the post discharge (0.05 ms and 4 ms). The exponents s were obtained by fitting the experimental data with a function of the form $I_{\mathrm{TALIF}} = A \cdot E_{\mathrm{L}}^{s}$.

absence of PMT space charge saturation, the decay time of the TALIF signal should be the natural lifetime of the excited state (15.5 ns and 35 ns for H and Kr respectively) since non radiative decay or line trapping are negligible in the present experimental conditions. If the anode current is saturated, the anode current intensity is no more proportional to the incident light level and the decay time of the TALIF signal becomes smaller than the natural lifetime. Fluorescence signals from Kr and atomic H were recorded. Figure 3 shows

the results of these measurements. Kr pressure of 23.7 Pa and 18.5 Pa were used for the measurements without and with the voltage-diver circuit, respectively. It is worth noting that a higher laser energy ($\sim$80 μJ, outside the quadratic dependence region) had to be set to demonstrate PMT saturation with Kr while PMT saturation was observed for H in the quadratic dependence region. H measurements were performed at a time $t = 0.2$ ms in the post discharge. An exponential fit of the data, excluding the laser pulse duration ($\sim$10 ns), was performed in order to get TALIF decay times as a function of the PMT slit opening. An example of fluorescence measurements and the fitting results are shown in Figure 3. By increasing the slit opening, the incident light flux onto the PMT was increased. As shown in Figure 3 (a and b), the intensity of TALIF signal was increased and the decay time remained at a constant value, close to the theoretical one, unless the incident light flux was too high leading to the saturation of the PMT signal. Based on the observed increase of the decay time at high photon flux (Figure 3b), the saturation started when using the 'non-tapered voltage-divider' when the slit opening was about 20 μm corresponding to a measured voltage in the range $120 - 200$ mV. It means that under these conditions, the TALIF signal should be maintained below $120 - 200$ mV by reducing the incident light level. This was limiting the measurement over a relatively small range of intensity and prevents measuring low atomic hydrogen density in the late post-discharge. Figure 3b shows that the PMT saturation threshold when using the 'tapered voltage-divider' circuit was reached at a higher photon flux with a slit opening between 80 and 160 μm, corresponding to about $\sim$500 mV (PMT saturation is shown by gray ellispe on Figure 3a). The PMT linearity range was thus improved and higher TALIF signal intensity could be recorded, thus improving signal-to-noise ratio and atomic detection limit.

3. Absolute density calibration

In order to obtain absolute density, the technique proposed by Goehlich et al [13] was used. The method is based on a comparison between the TALIF signal of the studied atomic species with the TALIF signal of a noble gas which has a two-photon resonance spectrally close to the transition investigated. A prerequisite for its applicability is that both TALIF excitations are performed with identical spatial, spectral, and temporal intensity distribution of the laser radiation. This removes the necessity of knowing the intensity distribution

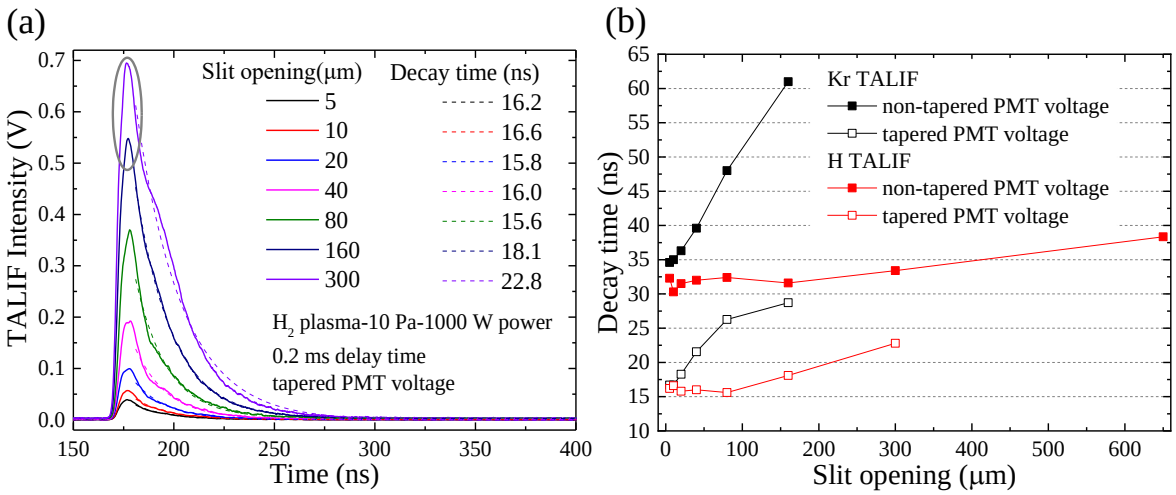

FIG. 3. (a) H TALIF signals versus slit opening (i.e versus photon flux) using a 'tapered voltage-divider' for the PMT dynode biasing. Appearance of PMT saturation is shown by the grey ellipse and is determined based on the measurement of TALIF decay times. (b) Kr and H TALIF decay times versus slit opening with and without a 'tapered voltage-divider' for the PMT dynode biasing. Krypton measurements were performed at ∼20 Pa without plasma. Hydrogen measurements were performed in a 1000 W, 10 Pa, 10 Hz pulsed plasma with a time delay $t = 0.2$ ms.

explicitly. The condition is best fulfilled if the two-photon resonances are spectrally as close as possible. For this reason, Kr was employed. The ratio of Kr to H TALIF signal intensities, $I_{\mathrm{TALIF,Kr}}/I_{\mathrm{TALIF,H}}$ is given by:

$$\frac{I_{\mathrm{TALIF,Kr}}}{I_{\mathrm{TALIF,H}}} = \gamma \frac{n_{\mathrm{Kr}}}{n_{\mathrm{H}}} \frac{\sigma^{(2)}_{\mathrm{Kr}}}{\sigma^{(2)}_{\mathrm{H}}} \left(\frac{I_{0,\mathrm{Kr}} \lambda_{\mathrm{Kr}}}{I_{0,\mathrm{H}} \lambda_{\mathrm{H}}} \right)^2 \frac{a_{32,\mathrm{Kr}}}{a_{32,\mathrm{H}}}, \tag{1}$$

where γ is the detection efficiency ratio for the two observed fluorescence wavelengths, n is the atom density, σ is the two photon absorption cross section, λ is the wavelength, I_0 is the laser energy, and a_{32} is the branching ratio of the fluorescence channel. The detection efficiency ratio γ between photon at 656 nm (H atom) and 826 nm (krypton) was determined using a blackbody (Luminance Radiance Standard from SphereOptics). Measurements resulted in a ratio equal to 0.73 ± 0.02.

For a gas at very low pressure and short lifetime excited states, no collisional deactivation occurs and the branching ratio a_{32} can be written as $a_{32} = A_{32} \cdot \tau_3$, where A_{32} is Einstein coefficient,τ_3 is the natural lifetime. The H atom density is then given by:

$$n_{\mathrm{H}} = \chi \frac{I_{\mathrm{TALIF,H}}}{I_{\mathrm{TALIF,Kr}}} \cdot \left(\frac{I_{0,\mathrm{Kr}}}{I_{0,\mathrm{H}}} \right)^2 n_{\mathrm{Kr}}, \tag{2}$$

where the factor χ is only composed of atomic and experimental constants,

$$\chi = \gamma \frac{A_{32,\mathrm{Kr}} \tau_{3,\mathrm{Kr}} \cdot \sigma^{(2)}_{\mathrm{Kr}} \cdot \lambda^2_{\mathrm{Kr}}}{A_{32,\mathrm{H}} \tau_{3,\mathrm{H}} \cdot \sigma^{(2)}_{\mathrm{H}} \cdot \lambda^2_{\mathrm{H}}}. \quad (3)$$

The ratio of the two-photon excitation cross sections was measured by Niemi et al [8] and the value is $\sigma^{(2)}_{\mathrm{Kr}}/\sigma^{(2)}_{\mathrm{H}} = 0.62$. Table I summarises the values of all parameters involved in the H atom density calibration via a Kr TALIF signal.

TABLE I. Parameters involved in the atomic hydrogen density calibration via krypton.

	Kr	H
λ (nm)	204.1954	205.1445
A_{32} (s^{-1})	$2.4 \cdot 10^7$ [14]	$6.45 \cdot 10^7$ [15]
τ (ns)	35.4 [9]	15.5 [7]
γ	0.73	
χ	0.43	

For calibration, Kr was injected into the plasma chamber at three different pressures and excited with a laser energy of 31 μJ. The detection system for krypton was identical as for H atom, except for the laser energy that was set to 376 μJ for H. Relative H atom density decay in 10 Hz, 10 % duty cycle, 1000 W input power, H_2 plasma was then calibrated (Figure 4). At the moment of the calibration, an alumina sample was installed in the chamber instead of the quartz sample. The sample material could affect the atomic density when compared to the full quartz situation, but the order of magnitude obtained here are still comparable to previous measurements realised in steady state plasma [5] since the sample surface was relatively small compared to surface area of the rest of the chamber walls. The absolute atom density at a time delay of 0.05 ms was $(9 \pm 1) \cdot 10^{19}$ m^{-3}. The absolute atom density in this experimental set-up and at the same pressure and RF power but in steady state was also determined by Ar actinometry with H_β line in H_2 + 5% Ar plasma using a Pyrex tube instead of a quartz one (Figure 14 of reference [5]). The result was $\sim 2.5 \cdot 10^{20}$ m^{-3} which compares quite well in term of order of magnitude to the present experiment given the slight differences between the experimental conditions (Pyrex tube instead of quartz tube, quartz sample instead of alumina sample, introduction of 5% argon, etc).

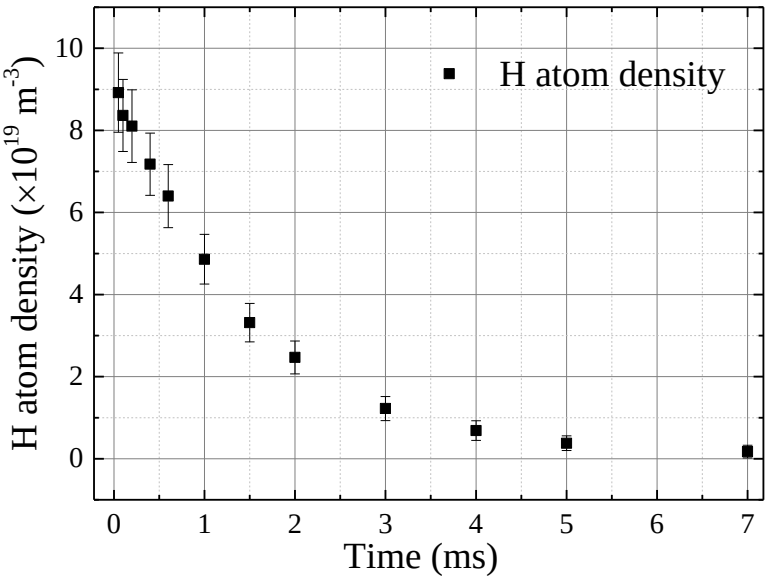

FIG. 4. Absolute H atom density in the post-discharge (10 Pa, 10 Hz, 10% duty cycle, 1000 W input RF power, pure H_2 plasma, 376 μJ laser energy)

4. Laser line width calibration

Figure 5a and b show the TALIF measured absorption profile for H and D atoms at different time delays, as well as the corresponding recorded laser energy. Each data point is an average of 50 TALIF signals normalised by the square of the average of the corresponding 50 recorded laser energies. The error bar of each point results from the standard deviation of the 50 averaged measurements. The solid curve is a Gaussian fit curve. The width of the Gaussian line is determined by the convolution of the Doppler broadening ($\Delta\lambda_{\mathrm{D}}$) given by the atomic temperature and the laser line width ($\Delta\lambda_{\mathrm{L}}$). H and D absorption profile full width at half maximum (FWHM) are given by:

$$\Delta\lambda_{\mathrm{m}}^2 = \Delta\lambda_{\mathrm{D}}^2 + \Delta\lambda_{\mathrm{L}}^2 \tag{4}$$

The laser line width is 1.2 pm at 615 nm (0.03 cm^{-1}) from manufacturer specifications giving a theoretical width of $\sim$0.4 pm at 205 nm (0.09 cm^{-1}). Using this laser line width leads to H and D temperature in the late post discharge higher than 1000 K and well above the expected value of 300 K (wall temperature remains close to room temperature). It shows that the laser was spectrally broader than expected preventing atomic temperature measurements unless laser line width was properly calibrated. Such an issue was already

reported in [16].

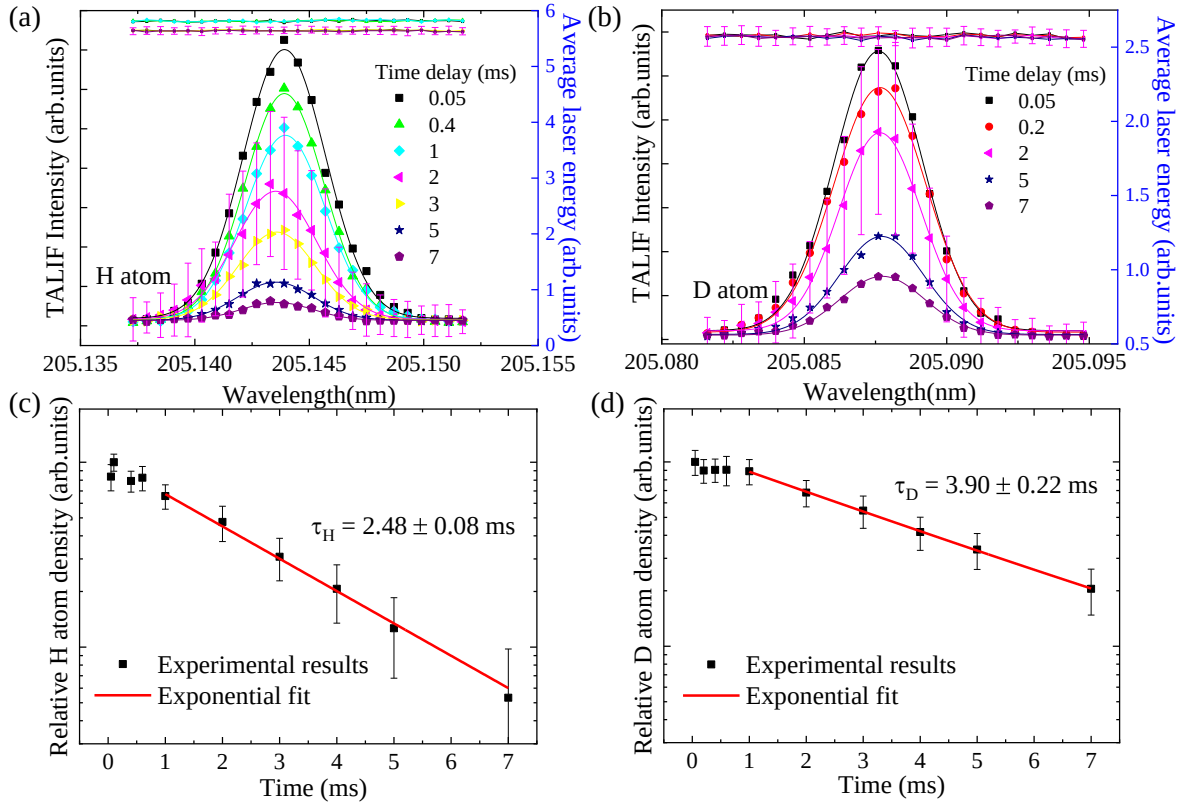

FIG. 5. TALIF measurement of H atom and D atom densities in 10 Pa, 10 Hz, 10% duty cycle, 1000 W input RF power H_2 (D_2) plasmas. The laser pulse energy recording during measurement is shown above the profiles (laser energy is about 370 μJ/pulse). (a) and (b) show the excitation spectrum at different time delays. (c) and (d) show the relative atom density as a function of time in the post discharge together with an exponential fit of the data. In (a) and (b), in order to avoid overlapping, the error bars are only shown for one time delay. The error bars correspond to the error of 50 averaged measurements for each wavelength.

Krypton is 42 times heavier than hydrogen and presents a narrow Doppler broadening at room temperature (∼0.27 pm) which is smaller than the laser (theoretical or real) line width. Its absorption profile should theoretically give the laser line width. However, the absorption profile measured by TALIF with a laser energy of 30 μJ at low pressure was found to be quite large (∼2.7 pm, not shown here) and was probably broadened by multiple transitions coming from sub-levels and/or isotopic shifts. Two other methods were thus used to determine laser line width.

The first one was proposed by Lamara et al [17]. It consists in measuring the absorption line of H and D atoms in discharges in H_2/D_2 mixture (see an example in Figure 8). H and D atoms are supposed to be in thermal equilibrium. Their excitation laser wavelengths are very close, and this gives the advantage of doing both absorption profile measurements with nearly identical laser properties. As H and D absorption profiles depend on the same two unknown parameters, the atomic temperature (assumed to be equal for H and D) and the laser line width, they can now be determined.

The absorption spectra of atomic hydrogen and deuterium in 50% H_2 + 50% D_2 plasma were recorded. The plasma was operated at 10 Pa, 10 Hz, 10% duty cycle, and 1000 W input power. Measurements were done with different laser energies at different time delays in the post-discharge (and thus different atomic temperatures). The normalised TALIF profiles were fitted with Gaussian functions in order to get the FWHM $\Delta\lambda_{\mathrm{mH}}$ and $\Delta\lambda_{\mathrm{mD}}$ from which the laser line width was determined. The deduced averaged laser apparatus function was 1.76 ± 0.1 pm. The uncertainty includes a contribution from the Gaussian fit accuracy and a contribution from the reproducibility of the experiment. The obtained value was lower than that obtained by krypton excitation spectrum ($\sim$2.7 pm).

In order to confirm the laser line width measured by the above method, a second method consisting in scanning the absorption spectrum of NO molecule at 205 nm was used. The NO molecule has ro-vibrationnal transitions between $A^2\Sigma$ and $X^2\Pi$ electronic state [18]. The single-photon absorption spectrum of NO molecule at room temperature was measured. For laser line width calibration, we have selected a transition with excitation wavelength and fluorescence at 205.28 nm ($A^2\Sigma^+(\nu = 2) \rightleftharpoons X^2\Pi(\nu = 0)$). The gas introduced in the vessel was a mixture of 99% Ar and 1% of NO. The gas pressure was set at 50 Pa which means the NO partial pressure was 0.5 Pa. Since the cross section is much higher for the single photon excitation than for the two-photon excitation, the laser injection was operated here without focusing. The fluorescence was focused on the photo-multiplier without any optical filter. The laser was scanned from 205.2802 nm to 205.2640 nm. The laser energy was 14 μJ. Due to its large mass, the Doppler broadening of NO molecule at room temperature is small ($\sim$0.46 pm) and cannot be resolved by the laser (theoretical bandwidth of 0.4 pm). Therefore, the Doppler broadening can be neglected and the line broadening of the excitation spectrum is related to the laser apparatus function (laser line width). Figure 6 shows the absorption profile of the selected NO transition. It was actually impossible to fit it by either a Gaussian

function, nor by the convolution of a Gaussian (FWHM 0.46 pm) with a Lorentzian. Only a Lorentzian function was able to fit correctly the spectrum.

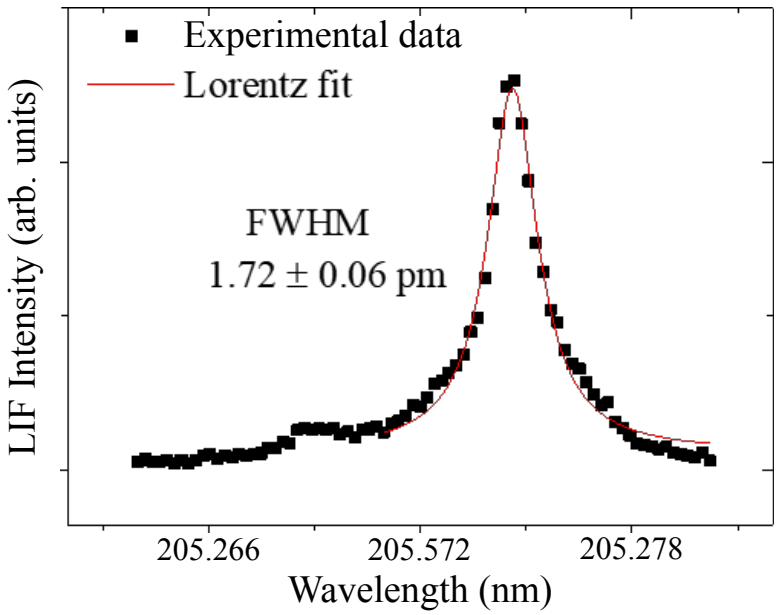

FIG. 6. Absorption spectrum of NO and corresponding fit by a Lorentz function. The laser pulse energy was 14 μJ, the laser wavelength was scanned from 205.2622 nm to 205.2462 nm, by steps of 0.0002 nm, 80 trigger events per step

The Doppler broadening was neglected and it was assumed that the Lorentzian width obtained is the laser line width. The deduced laser broadening was 1.72 ± 0.06 pm which agrees very well with the broadening obtained from the H and D scan. This confirmed that the laser line width was around 1.7 pm at 205 nm.

Using this value for the laser line width, time resolved measurements of the atomic temperature by performing Gaussian fits of the absorption profiles were possible. The atomic temperature was observed to decrease rapidly during the first millisecond of the post discharge. However the errors on the temperature measurement were rather large and fluctuations up to $\sim$100 K were observed. The reasons behind these observed temperature fluctuations are still unknown. Possible explanations are small changes of the laser line width with time and insufficient averaging resulting in a decrease accuracy of the Gaussian fits. Despite these fluctuations, it can still be deduced from the measurements that atomic temperatures are more or less in thermal equilibrium with the walls ($\sim$300 K) after about 1 ms in the post discharge. One representative measurement is given in Figure 7.

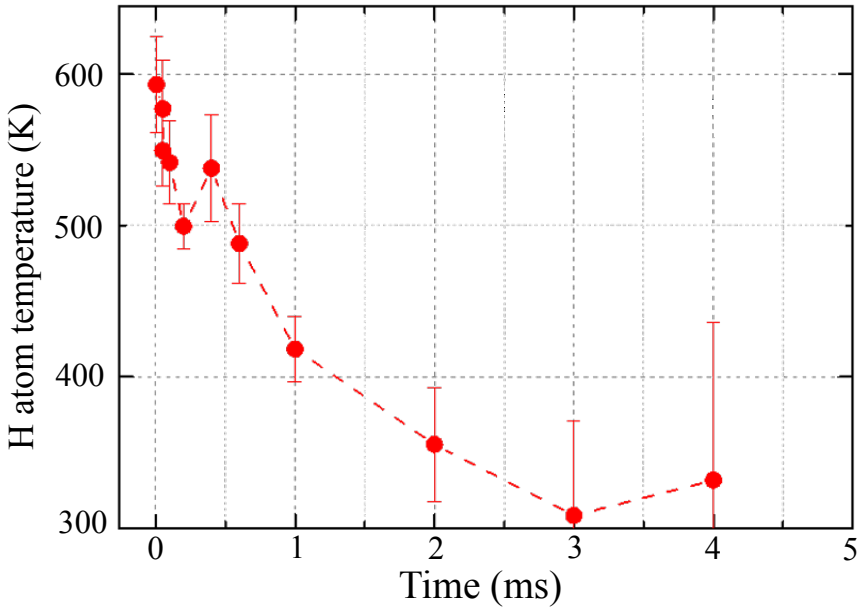

FIG. 7. H atom temperature decay in the post-discharge. Pure H_2 plasma pulsed at 10 Hz, 10% duty cycle and 1000 W input power.

III. RESULTS AND DISCUSSION

A. TALIF Measurements

The relative density of atomic hydrogen and deuterium in the post-discharge was evaluated by calculating the area under the curve of the absorption profile. Figure 5c and 5d show relative atomic hydrogen and deuterium density in the post discharge. The error bar was the propagation of errors in Figure 5a and 5b. A decay of atomic density over one order of magnitude was observed before the signal came into noise. One can see that the signal in the early afterglow was not following a monotonic decay. This is possibly due to gas cooling during the first millisecond impacting H radial profile and more generally speaking, neutral density distribution inside the plasma [19, 20]. Therefore, only data points acquired at time higher than 1 ms were used to determine surface loss probabilities. If one excludes the first millisecond, the atomic decays were indeed quite accurately described by an exponential decay function ($y = y_0 + A_1 e^{(-t/\tau)}$) with a time constant τ lower for H than D ($\tau_H < \tau_D$).

In order to compare H atom and D atom surface loss probabilities under the exact same plasma conditions, H and D atom decay times in the post discharges of H_2-D_2 (50%-50%) plasma were measured. Figure 8 shows the results. The laser pulse energy was ~270 μJ for

this measurement. If one excludes the first millisecond, the decays were again exponential with $\tau_H < \tau_D$.

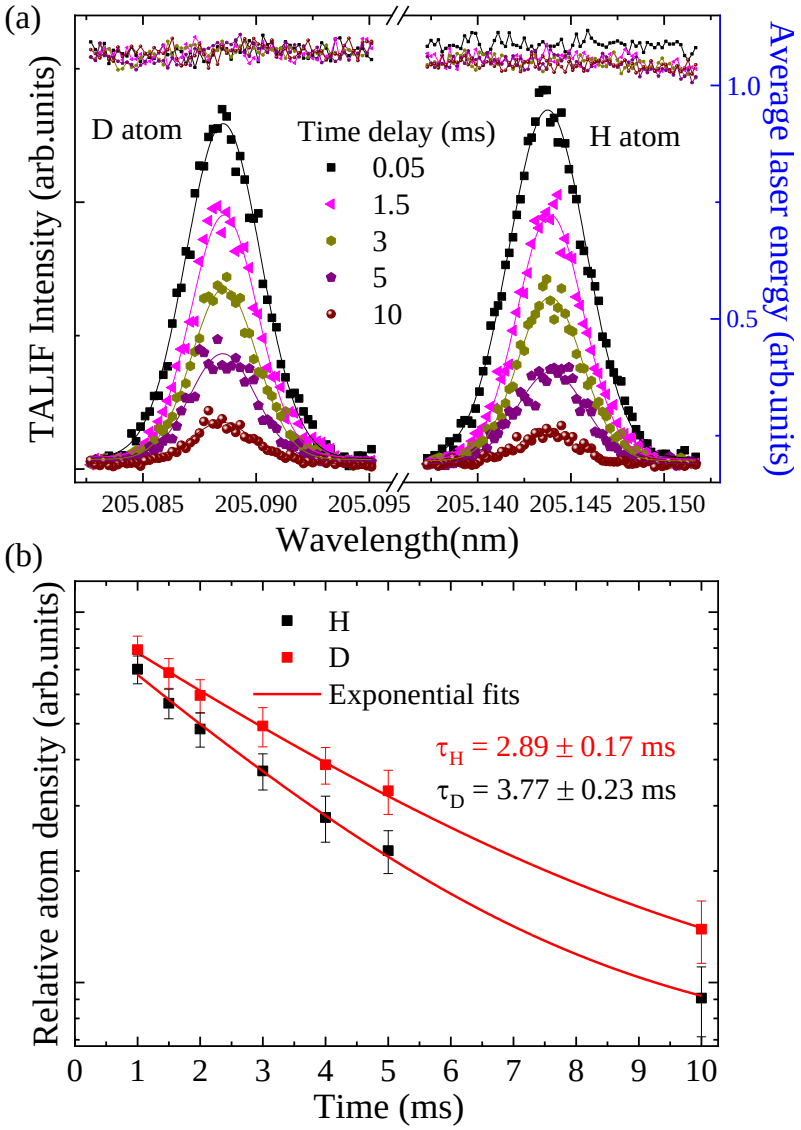

FIG. 8. (a) H and D atom absorption profiles in H_2/D_2 plasmas (1:1 mixture, 1000 W, 10 Pa, 10 Hz, 10% duty cycle) at different times during the post discharge. The laser pulse energy recorded during the measurement of the profiles is shown above the profiles. (b) Relative atom density as a function of time during the post discharge. Fitted lines were obtained using exponential decay functions.

H atom decay was also measured in 10 Pa, 1 Hz, 5% duty cycle, 1000 W RF input power plasmas, for comparison purposes with previous measurements. The laser pulse energy was 225 μJ. Figure 9 shows the TALIF measurements. Excluding the first millisecond, the decay

was also exponential.

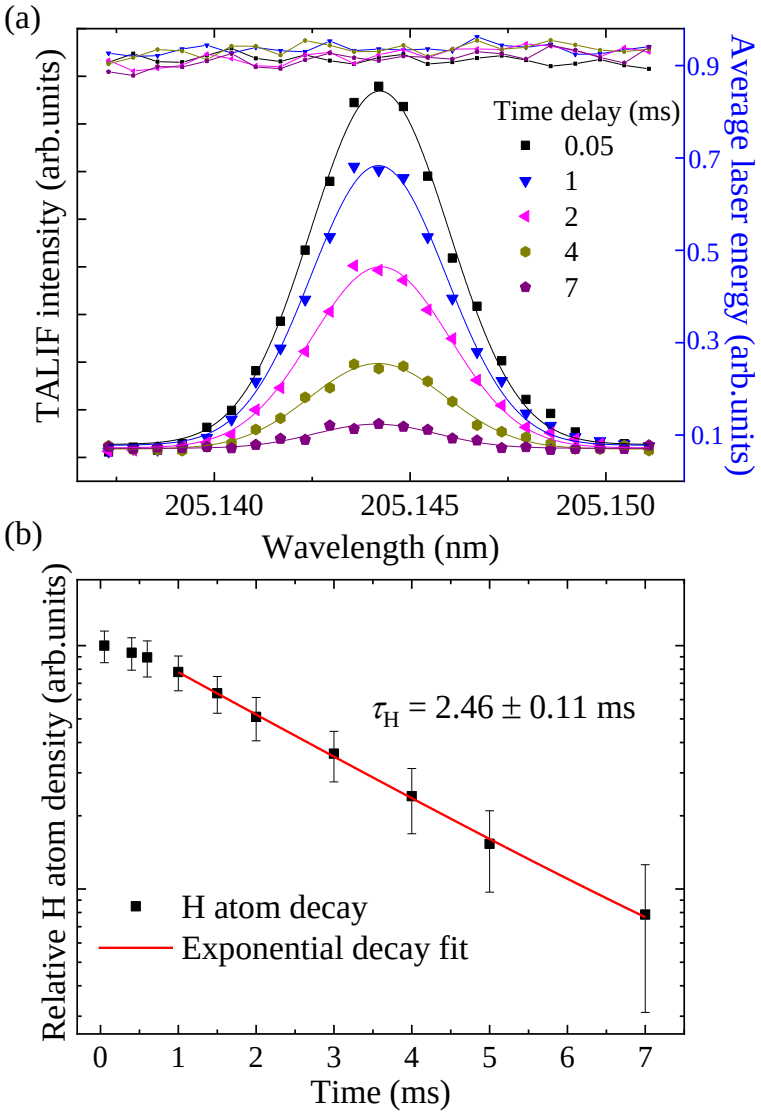

FIG. 9. a) H atom absorption profiles in H_2 plasma (1000 W, 10 Pa, 1 Hz, 5% duty cycle) at different times in the post discharge. The laser pulse energy recorded during the measurement of the profiles is shown above the profiles. (b) Relative atom density as a function of time in the post-discharge. The fitted line was obtained assuming an exponential decay.

B. Surface loss

The H/D atom loss probability on surface was determined from the measurement of the atom density [H], [D] as a function of time in the post discharge. Atomic reactions on silica

like surface are well described in [21]. Briefly, gaseous atoms can be lost at the surface through chemisorption, which is creating and adsorbed atom, direct recombination between a gaseous atom and an adsorbed atom (Eley-Rideal reaction), and recombination between a diffusing atom on the surface and a chemisorbed atom. Eley Rideal process is always a first order process with respect to the gaseous atomic loss (i.e loss rate is proportional to the gaseous atomic density) while Langmuir-Hinshelwood loss can be second order in the limit of low temperature (which is not corresponding to the situation studied in this paper). It is not easy to determine which mechanism is dominating in a given experimental condition but recent measurements in oxygen plasma demonstrated that oxygen atomic loss on Pyrex obviously occurs through the Eley Rideal mechanism at room temperature at least for pressure above 100 Pa [22]. For lower pressure the increasing influence of ion bombardment did not permit to conclude on the dominating mechanism. Anyway, for all the reasons mentioned in this paragraph, it is a reasonable assumption to consider that the atomic surface loss probability is independent on the atomic density giving a first order atomic loss rate as described in the next paragraph.

As soon as the plasma pulse is switched off, because of the very fast cooling of the electron temperature, there is no more production of atoms by electron impact. As atomic loss by three body recombination in the plasma volume is much slower than the observed decay time, the equation governing atomic kinetics in the post discharge reads as:

$$\frac{\partial[\mathrm{H}]}{\partial t} - D\vec{\nabla}^2[\mathrm{H}] = 0. \tag{5}$$

If the diffusion coefficient D is constant in time and space the solution to this equation is an infinite sum of eigenmodes:

$$[\mathrm{H}](t,\vec{r}) = [\mathrm{H}]_0 \sum_{i=0}^{\infty} \psi_i(\vec{r}) \exp\Big(-\frac{t}{\tau_i}\Big). \tag{6}$$

The fundamental mode might not describe properly the H atom density spatial profile in a plasma source where significant heating such as the one used in the present study. Indeed, at constant pressure, the "hottest" plasma region might be depleted in neutral atoms [19]. However, in the afterglow, it is usually assumed that the H atom density is accurately represented by the fundamental mode since the higher order modes are quickly damped once the gas has cooled down:

$$[\mathrm{H}](t,\vec{r}) = [\mathrm{H}]_0\psi_0(\vec{r})\exp\Big(-\frac{t}{\tau_0}\Big). \tag{7}$$

The function $\psi_0(\vec{r})$ depends on the geometry of the plasma chamber and on the boundary conditions (i.e. on the loss probability at the wall) and can be easily determined for simple geometries. As mentioned previously, the plasma region in the present experiment has a simple cylindrical geometry. The characteristic time of the first order mode depends on the loss probability at the wall [23] and can be approximated by:

$$\tau_0 = \frac{\Lambda_0^2}{D} + \frac{V}{A}\cdot\frac{2(2-\gamma_\mathrm{s})}{\gamma_\mathrm{s}\langle v\rangle}, \tag{8}$$

where A is the area of the wall surface, V is the chamber volume, $\langle v\rangle$ is the H atom thermal velocity, γ_s is the surface loss probability and Λ_0 is the diffusion length determined by the reactor geometry and dimensions.

The H atom density decrease obtained experimentally was fitted by an exponential function and the characteristic time obtained were used to determine the loss probability at the wall from Eq. 8. Let us note that this approach gives an average loss probability on all surfaces in contact with the plasma. Since all surfaces in contact with plasma are quartz surfaces in the present study, it allowed us determining atomic loss probability on quartz.

Eq. 8 is valid only if the diffusion coefficient is constant in time and space. However, under our experimental conditions the gas was quite hot during the plasma pulse [5] and the diffusion coefficient was varying with time in the post discharge due to gas cooling. For this reason, as previously stated, data acquired at time shorter than one millisecond were disregarded for the determination of surface loss probability. The diffusion coefficient was calculated as follows:

$$D = \frac{\pi}{8}\lambda\langle v\rangle, \tag{9}$$

with the mean free path $\lambda = \frac{1}{\sigma N}$, N being the neutral gas density and $\sigma = 2.2\cdot 10^{-19}$ m^2 the momentum transfer cross section given by Krstic and Schultz [24]. They demonstrated that the cross section is identical for hydrogen, deuterium and tritium whatever the collision partners (H with H_2, H with HD, D with D_2, etc).

Exponential fits of atomic decays are presented on Figure 5, Figure 8 and Figure 9. The corresponding decay times are given in Table II together with the deduced loss probability for both hydrogen and deuterium (from Eq. 8). The obtained loss probabilities are for atoms

at ∼300 K interacting with a quartz surface at ∼300 K. In his article [23] Chantry evaluated the error made by using the approximate analytical solution (Eq. 8) to determine decay time, as a function of container aspect ratio and surface loss value. The error made under our experimental conditions can be estimated thanks to Figure 4 of reference [23] (cylinder with an aspect ratio of 2, diffusion of H atoms with a loss probability at the wall of ∼2%) and leads to an overestimation of the loss probability by 6% at maximum. The loss probabilities presented in Table II have been corrected accordingly.

TABLE II. Decay time constants for H and D obtained by exponential fit of the experiments and the corresponding surface loss probabilities

	τ_{H} (ms)	τ_{D} (ms)	$\gamma_{\mathrm{H_{corr}}}$	$\gamma_{\mathrm{D_{corr}}}$
Pure gas 10 Hz	2.48 ± 0.08	3.90 ± 0.22	0.019 ± 0.001	0.017 ± 0.001
H_2:D_2 mixture 10 Hz	2.89 ± 0.17	3.77 ± 0.23	0.016 ± 0.001	0.018 ± 0.001
Pure gas 1 Hz	2.46 ± 0.11	-	0.019 ± 0.001	-

C. Discussion

1. Atomic surface loss

As discussed in the introduction, many measurements of hydrogen surface loss probabilities on various surfaces can be found in the literature but only a part of them deal with glass surfaces [25–31], and to the best of our knowledge none of them consider deuterium atoms. Furthermore, for any kind of material, results are generally scarce and can span over two or three orders of magnitude [27]. This is because atomic surface loss strongly depends on surface state [32] which is not controlled under plasma exposure. Surface state depends on surface temperature, positive ion flux, positive ion energy, atomic flux, base pressure, gas purity, etc. Most of these parameters depend on experimental conditions (pressure, power, etc). Furthermore atomic surface loss might also depends on plasma parameters such as the atomic temperature in the vicinity of the wall as demonstrated recently [22]. As a consequence, comparisons between different plasma reactors, with different pressure or power conditions are rather difficult to perform. However, there are few general trends that can be extracted from the literature. First, surface loss probabilities are usually higher

when surfaces are directly exposed to the plasma (measurement in the discharges or in the post discharges) than when they are not (measurement in flowing afterglow) [33]. This is probably due to the very different surface states obtained when surfaces are exposed to positive ion bombardment which are thought to have a cleaning effect. Adsorbed water molecules that poison atomic recombination at surfaces are for instance probably desorbed due to ion bombardment [34]. H surface loss probabilities on glass surfaces ranging from 10^{-5} to $8 \cdot 10^{-2}$ can be found in the literature [27]. If measurements in spatial afterglow are excluded, measurements still range between $\sim 10^{-4}$ and $\sim 10^{-2}$ [26, 27]. Some pressure resolved studies [35–39] seem to indicate that H atom loss probabilities on aluminium and stainless steel are higher in low-pressure high density plasma sources, such as the one used in the present study, than in higher pressure sources. This has been summarised by Sode et al [40]. Booth et al have shown for oxygen atoms loss on Pyrex that two pressure regimes might exist [22]. A high pressure regime (above 100 Pa in their experimental device) where atomic loss probability variations are fully explained by the atomic temperature close to the wall, and a low pressure regime with an increase of loss probability that cannot be explained by the atomic temperature. This increase might be due to an increasing influence of positive ion bombardment on the walls due to a decrease of sheath collisionality at lower pressure. In this study, measurements were limited to a minimum pressure of about 27 Pa. However, it shows that for a proper comparison with existing data, it is preferable to select similar pressure ranges and, more generally speaking, similar experimental conditions. In that sense, measurements of H atomic loss on Pyrex done by Samuell et al [27, 31] are the closest to the present ones. They found a value of $8 \cdot 10^{-2}$ at about 10 Pa and 800 W RF power in a high density helicon plasma source. Even if the pressure and the power density were different in both studies, positive ion flux and positive ion energy were of the same order of magnitude, giving relevance to the comparison. Both measurements give surface loss probabilities much higher than measurements done at higher pressure or in flowing conditions, confirming that in low-pressure high density hydrogen plasmas the atomic loss probability on glass is rather high.

2. *Isotopic effects in atomic production and losses*

It can be noticed from Figure 5, Figure 8, and Figure 9 that deuterium atomic decay time is noticeably higher than the hydrogen one. However, Table II shows that atomic surface loss probabilities are similar for both isotopes, both in pure gas and H:D mixture. This demonstrates that there is no isotopic effect with regards to the atomic surface kinetics, but there is an isotopic effect on atomic loss. The faster decay time (which means higher loss rate) of hydrogen atoms is explained by its lower mass giving faster diffusion towards the wall (first term in Eq. 8) and higher flux to the wall (thermal velocity in the second term). The latter contribution is the most important, the former contributing only to $\sim$15% to the decay time.

Despite identical surface loss probabilities, the lower loss rate should lead to higher atom density in D_2 plasmas compared to equivalent H_2 plasmas if the production mechanisms were identical. In H_2:D_2 (50%-50%) plasma it has been observed on the contrary that H TALIF signal was slightly higher or equal to D one (H to D TALIF ratios were between 1 and 1.3). Two photon absorption cross sections differences between hydrogen and deuterium are insignificant and can be disregarded [41] for data analysis. Therefore, it is worth discussing isotope effects on atom production mechanisms in the context of the present paper. Three production mechanisms are considered and their isotopic effects are discussed: i) electron impact dissociation of molecules is expected to be the predominant mechanism for atomic production and therefore must be considered with attention, ii) electron attachment on vibrationally excited molecules producing a negative ion and an atom is not expected a priori to be a major source of atomic species but is known to demonstrate a strong isotopic effect, iii) finally, production of atomic species through positive ion loss is also considered as it might be of importance in a high density plasma source.

Dissociation by electron impact is first considered. Due to the complexity of the dissociation process, there are only a few available data for hydrogen dissociation cross sections and even fewer for deuterium [42, 43]. H_2 and D_2 dissociation at low electron energy (below $\sim$15 eV) proceeds only through the excitation of the pre-dissociative $b^3\Sigma_u$ state. All references report a maximum cross section for this process at energy in the range 12-18 eV, with a value between 0.3 and $0.8 \cdot 10^{16}$ cm^2 [44–49], and close to $0.5 \cdot 10^{16}$ cm^2 for the most recent references [47–49]. At energy above the maximum of H_2 ($b^3\Sigma_u$ state) excitation cross

section, contributions from other excited electronic states arise and, depending on the references, dominate [42] or significantly participate [46] to the H_2 total dissociation cross section. There is no measurement of this contribution for D_2. Recent calculations [44, 46] consider the excitation of $b^3\Sigma_u$ state (and therefore the dissociation of the molecule) for H_2 and D_2 from threshold to hundreds of eV. At high energy H_2 and D_2 dissociation cross sections are found to be identical while, at energy between threshold and 12 eV, the H_2 cross section is higher by a factor varying from 1 to 10. These results are in contradiction with Celiberto et al [49] who found higher cross section for D_2 at high energy, and in contradiction with Trevisan and Tennyson [48] who found a cross section about two times higher for D_2 at low energy (below 12 eV) [43, 48]. The disagreement at high energy between different studies does not matter too much since in a low electron temperature plasma source, and for a process with a maximum cross section below 20 eV, the contribution of high energy electron to dissociation can be neglected. However, the differences at low energy have a strong effect on the calculation of the dissociation rate.

We have calculated the dissociation rate coefficients of H_2 and D_2 for a Maxwellian electron distribution using the most recent cross sections of Refs. [44, 46] . They are plotted as a function of the electron temperature T_e in Figure 10 [50]. Without the quartz tube (stainless steel chamber) and in DC mode, we measured a low electron temperature of 0.8 eV at 10 Pa and 1000 W, 5 cm above the wafer [51]. A measurement was also performed with a Pyrex tube equipped with a large enough hole to allow Langmuir probe introduction in the plasma, and an almost similar electron temperature of 0.7 eV [10] was found. However, due to the relatively high pressure considered in the present study, the electron temperature might not be uniform in the plasma. Axial measurements of electron temperature have been performed at 10 Pa and 1000 W in H_2 in another cylindrical plasma reactor equipped with a similar 3 turns RF antenna. The main differences were the chamber radius (10 cm versus 8 cm) and the walls made of stainless steel instead of quartz. While the different surface over volume ratio is not affecting too much the electron temperature (as predicted by simple global plasma modelling [52, 53]), the difference in chamber walls might lead to different plasma composition because of the different surface losses and therefore different electron temperature. Thus, the most interesting information is the observed vertical gradient rather than the absolute electron temperature values. The electron temperature has been found to increase from 0.8 eV to 1.45 eV at 5 cm from bottom and 2.45 eV at 10 cm from bottom. An

extrapolation of the measurement to 14 cm gives an axially averaged electron temperature at 10 Pa equal to 2.4 eV well above the 0.8 eV measured at bottom and still well above measurement at 5 cm from the bottom. It appears therefore that a spatial distribution of T_e in the plasma reactor has to be considered to study H/D production mechanisms. A simple volume averaged analysis equalling hydrogen production and loss rate tells that a production rate as high as 10^{23} $m^{-3}s^{-1}$ is required to account for a H density of $3 \cdot 10^{20}$ m^{-3} (Figure 4) with H loss frequency of $\sim$350 s^{-1} ($1/\tau_H$, Table II). Figure 10 presents dissociation production rates (k_{diss} n_e [H_2]) computed using an electron density of $1 \cdot 10^{17}$ m^{-3} and a H_2 density of $2.4 \cdot 10^{21}$ m^{-3} (10 Pa and 300 K). Dissociation production rate reaches 10^{23} $m^{-3}s^{-1}$ at an electron temperature of 2.5 eV, or 5 eV if ones takes into account a higher average gas temperature (900 K at 10 Pa [5]) and a lower H_2 density.

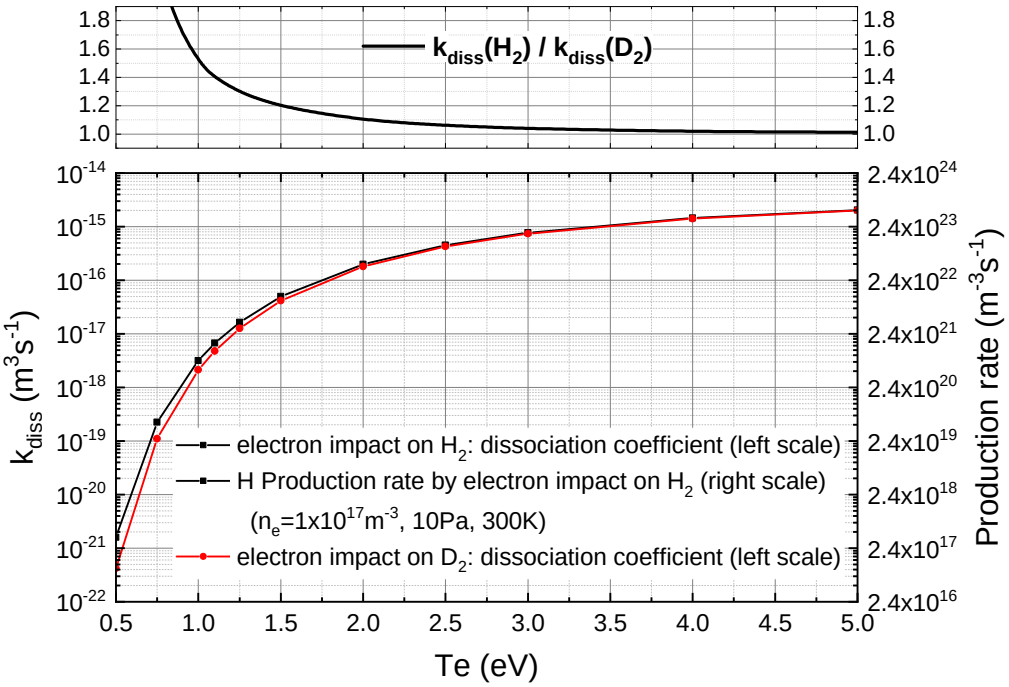

FIG. 10. Electron impact dissociation of H_2 and D_2 as a function of the electron temperature T_e: dissociation coefficients (left scale) calculated for Maxwellian electron distribution functions and H production rate (right scale) given for an electron density of $1 \cdot 10^{17} m^{-3}$ and a H_2 density of $2.4 \cdot 10^{21}$ m^{-3} (10 Pa and 300 K). On top is given the ratio between H_2 and D_2 dissociation coefficients

In order to get a higher or equivalent H density (compare with D one) while H loss rate is larger by a factor of about 1.3, a dissociation coefficient larger by at least a factor of 1.3 for hydrogen is required. From Figure 10 this can only occur for electron temperature below 1-1.5 eV. At such low temperature the production rate is too low to have a significant impact on H and D population. Furthermore, as discussed previously the average electron temperature is probably much higher than 1 eV in the present plasma source. At higher electron temperature the higher cross sections for H at low energy ([44] and [46]) have less importance and the dissociation coefficient ratio is approaching unity. Let us note however, that at 2.5 eV, when the production rate is reaching the expected value under our experimental conditions, the H dissociation coefficient is still 5% higher than D one. This account for a small isotopic effect in atom production. Note however that the 5% difference between the dissociation coefficients probably falls within uncertainties in the knowledge of the dissociation cross sections. Finally, it worth mentioning that even if the H atom density is measured in the region of low electron temperature, it is reflecting the global production mechanisms in the whole plasma source. Indeed, fast diffusion and low surface loss rate tend to equalize the H density throughout the reactor volume.

Dissociative attachment of an electron on a vibrationally excited molecule is now considered. Dissociative attachment of an electron on a vibrationally excited hydrogen or deuterium molecule is producing one negative ion and one atom. It is known to present strong isotope dependence, the cross sections for hydrogen being higher by orders of magnitude than those of deuterium [51, 54–56]. Based on cross sections of [49] (slightly lower than the original cross sections of Ref. [57]) we have calculated dissociative attachment rate for a vibrational temperature of 3300 K [5], a hydrogen density of $2.4 \cdot 10^{21}$ m^{-3} (10 Pa and 300 K), an electron density of $1 \cdot 10^{17}$ m^{-3} and rotationless vibration states from $\nu = 0$ to $\nu = 5$. The maximum production rate is $2 \cdot 10^{20}$ m^{-3}s^{-1}, far away from the required production rate.

Finally, atomic production through positive ion loss is considered. At 10 Pa the dominant positive ion is most probably H_3^+ due to very efficient conversion mechanism of H_2^+ by collision with H_2: $H_2^+ + H_2 \rightarrow H_3^+ + H$. This reaction creates a hydrogen atom. Furthermore, loss mechanisms of H_3^+ (or D_3^+) ion create from one to three atoms [19]. If we assume for the sake of simplicity that all H_2^+ ions are converted into H_3^+ then the production rate of H atoms through this mechanism is given by the ionisation rate of H_2 (multiplied by a factor from 2 to

4 to take into account ion loss). With a hydrogen molecular density of $2.4 \cdot 10^{21}$ m^{-3} (10 Pa and 300 K) and an electron density of $1 \cdot 10^{17}$ m^{-3}, this production rate reaches 10^{22} m^{-3}s^{-1} at $T_e = 3$ eV and 10^{23} m^{-3}s^{-1} at $T_e = 5$ eV (cross sections from [58]). Therefore, between 3 and 5 eV this mechanism could contribute in a non-negligible manner to the atomic production. Isotopic effect in molecule ionisation or in H_2^+/D_2^+ ion conversion could therefore influence the balance between H and D atoms in the discharge. Isotopic effect in electron impact ionization of hydrogen molecules is documented in particular in Ref. [43]. For electrons from threshold (16 eV) up to 25 eV the deuterium electron impact total ionization cross section (dissociative and non-dissociative ionisation) is slightly higher than the hydrogen one (by a maximum factor of 1.15) and cannot be at the origin of a higher H density. Above 25 eV there is no more isotope dependence. Concerning isotopic effect in H_2^+/D_2^+ ion conversion into H_3^+/D_3^+ we are not aware of any publication and cannot conclude. Let us note that ion conversion could contribute by few percent or few tens of percents to atomic production, and therefore would most probably do not have any major isotopic effect. This point could only be verified with the development of a dedicated model.

This simple analysis shows that for electron temperature around 2-3 eV, which is the average value expected in the present conditions, there is no obvious isotopic effect in H and D production mechanisms. On the contrary we have measured a clear isotopic effect in atomic loss which should lead to higher D than H densities which was not observed. A complete model, preferentially including vibrational states, would be required to discuss in details the isotopic effects and to explain these experimental observations. Besides, more experiments would be necessary to validate the set of cross sections to be used. Dissociation cross sections could be investigated for instance by using the positive column of a higher pressure DC discharge where the electron temperature is homogeneous and in the appropriate range ($\sim$2 eV), such as it has been carefully done recently for the dissociation cross sections of CO_2 [59].

An important outcome of the present work is that the same surface loss probability was measured for H and D on quartz. Lamara et al [17], and other authors previously [60, 61], found H and D densities in plasmas corresponding to the H_2:D_2 mixture ratio. Lamara et al suggested that D surface loss probability was higher than the H one, but their suggestion was based on Trevisan and Tennyson [48] dissociation cross sections demonstrating higher values for D_2 than H_2. However, not all dissociation cross section sets are demonstrating

such effect and our work is showing that deuterium surface loss probability is not higher than the H one. Galante et al [62] suggested that the higher atomic density they measured in D_2 helicon plasmas with respect to H_2 plasmas was due to the mass difference (and therefore to a slower diffusion and a lower flux to the wall). This is consistent with the results obtained here showing smaller D decay time.

IV. CONCLUSION

In this paper we have measured hydrogen and deuterium atomic loss probabilities on quartz in low pressure high density inductively coupled plasma source. The surface loss probability found for H is much higher than the value found at higher pressure in good agreement with recent measurements in similar experimental conditions [27, 31]. In pure hydrogen/deuterium gas or in mixture gas, no isotopic effect on surface kinetics has been observed and the surface loss probability of H and D were found to be almost identical and equal to $\sim$0.018 (1.8%). However, despite the lack of difference in surface loss probability, there is a net isotopic effect on surface loss rate due to the difference in mass between the isotopes leading to higher diffusion to the wall and higher flux at the wall for hydrogen atoms (the hydrogen atoms are lost faster than the deuterium ones).

Based on this isotopic difference and on the comparison between H and D TALIF signals, we discussed the atomic production mechanism isotopic effects. Three production mechanisms were considered, namely dissociation of the molecule by electron impact, dissociation by electron attachment, and ion conversion. Based on existing cross sections and on simple volume averaged analysis, no clear isotopic effect could been demonstrated for an electron temperature range relevant for the present study.In our case, a clear isotopic effect in atom loss was measured but with almost equivalent H and D atom density. Thus, a definite conclusion would require further analyses and vibrational state resolved modelling for both hydrogen and deuterium.

ACKNOWLEDGMENTS

This work has been carried out within the framework of the EUROfusion Consortium and has received funding from the Euratom research and training programme 2014-2018

and 2019-2020 under grant agreement No 633053. The views and opinions expressed herein do not necessarily reflect those of the European Commission. This work was carried out within the framework of the French Federation for Magnetic Fusion Studies (FR-FCM) and received some funding from FR-FCM. Financial support was received from the French Research Agency (ANR) under grant ANR-06-BLAN-0008 CAMITER and from the PACA county (project FORMICAT 2008). XY received financial support from the program of China Scholarships Council (No. 201304910334). GC and XY would like to thank Jean Paul Booth for fruitful discussions and NO molecule TALIF measurements. Alexandre Escarguel and Pierre David are acknowledged for their help in detection efficiency determination. LC acknowledges the support of the Natural Sciences and Engineering Research Council of Canada (NSERC), RGPIN-2019-04333.

[1] G. Cunge, D. Vempaire, R. Ramos, M. Touzeau, O. Joubert, P. Bodard, and N. Sadeghi, Radical surface interactions in industrial silicon plasma etch reactors, Plasma Sources Sci. Technol. **19**, 034017 (2010).

[2] G. Federici, C. H. Skinner, J. N. Brooks, J. P. Coad, C. Grisolia, A. A. Haasz, A. Hassanein, V. Philipps, C. S. Pitcher, J. Roth, *et al.*, Plasma-material interactions in current tokamaks and their implications for next step fusion reactors, Nucl. Fusion **41**, 1967 (2001).

[3] G. Matthews, Plasma detachment from divertor targets and limiters, J. Nucl. Mater. **220**, 104 (1995).

[4] R. Pitts, X. Bonnin, F. Escourbiac, H. Frerichs, J. Gunn, T. Hirai, A. Kukushkin, E. Kaveeva, M. Miller, D. Moulton, *et al.*, Physics basis for the first iter tungsten divertor, Nuclear Materials and Energy , 100696 (2019).

[5] J. Krištof, A. Annušová, M. Anguš, P. Veis, X. Yang, T. Angot, P. Roubin, and G. Cartry, Diagnostics of low-pressure hydrogen discharge created in a 13.56 mhz rf plasma reactor, Phys. Scr. **91**, 074009 (2016).

[6] K. Suzuki, K. Konishi, K. Nakamura, and H. Sugai, Effects of capacitance termination of the internal antenna in inductively coupled plasma, Plasma Sources Sci. Technol. **9**, 199 (2000).

[7] Anon, NIFS database (2017).

[8] K. Niemi, V. Schulz-Von Der Gathen, and H. Döbele, Absolute calibration of atomic density

measurements by laser-induced fluorescence spectroscopy with two-photon excitation, J. Phys. D: Appl. Phys. **34**, 2330 (2001).

[9] M. Boogaarts, S. Mazouffre, G. Brinkman, H. van der Heijden, P. Vankan, J. Van der Mullen, D. Schram, and H. Döbele, Quantitative two-photon laser-induced fluorescence measurements of atomic hydrogen densities, temperatures, and velocities in an expanding thermal plasma, Rev. Sci. Instrum. **73**, 73 (2002).

[10] X. Yang, *Study of the hydrogen-tungsten interaction for fusion: measurement of the atomic reflection coefficient by laser spectroscopy*, Ph.D. thesis, Aix-Marseille Université (2017).

[11] G. Sultan, G. Baravian, and J. Jolly, Resonant three-photon ionization and two-photon laser-induced fluorescence of atomic oxygen in a discharge and post-discharge, Chem. Phys. Lett. **175**, 37 (1990).

[12] J. E. Goldsmith, Two-photon-excited stimulated emission from atomic hydrogen in flames, Journal of the Optical Society of America B **6**, 1979 (1989).

[13] A. Goehlich, T. Kawetzki, and H. Döbele, On absolute calibration with xenon of laser diagnostic methods based on two-photon absorption, The Journal of chemical physics **108**, 9362 (1998).

[14] R. Chang, H. Horiguchi, and D. Setser, Radiative lifetimes and two-body collisional deactivation rate constants in argon for kr (4 p 55 p) and kr (4 p 55 p') states, The Journal of Chemical Physics **73**, 778 (1980).

[15] W. Wiese, Atomic transition probabilities and lifetimes, in *Progress in Atomic Spectroscopy* (Springer, 1979) pp. 1101–1155.

[16] D. B. Elliott, *Two Photon Absorption Laser Induced Fluorescence for Fusion Class Plasmas*, Ph.D. thesis, West Virginia University (2016).

[17] T. Lamara, R. Hugon, and J. Bougdira, Influence of gas temperature on the loss mechanisms of h-atoms in a pulsed microwave discharge identified by time-resolved lif measurements, Plasma Sources Sci. Technol. **15**, 526 (2006).

[18] R. W. B. Pearse and A. G. Gaydon., *The Identification of Molecular Spectra*, edited by Chapman and L. Hall (J. Wiley & Sons, 1941).

[19] L. Liard, A. Aanesland, and P. Chabert, Dynamics of neutral gas depletion investigated by time-and space-resolved measurements of xenon atom ground state density, J. Phys. D: Appl. Phys. **45**, 235201 (2012).

[20] F. Gaboriau and J. Boeuf, Chemical kinetics of low pressure high density hydrogen plasmas: application to negative ion sources for iter, Plasma Sources Sci. Technol. **23**, 065032 (2014).

[21] V. Guerra, Analytical model of heterogeneous atomic recombination on silicalike surfaces, IEEE Transactions on plasma science **35**, 1397 (2007).

[22] J.-P. Booth, O. Guaitella, A. Chatterjee, C. Drag, V. Guerra, D. Lopaev, S. Zyryanov, T. Rakhimova, D. Voloshin, and Y. Mankelevich, Oxygen (3p) atom recombination on a pyrex surface in an O_2 plasma, Plasma Sources Sci. Technol. **28**, 055005 (2019).

[23] P. Chantry, A simple formula for diffusion calculations involving wall reflection and low density, J. Appl. Phys. **62**, 1141 (1987).

[24] P. Krstic and D. Schultz, Elastic and inelastic collision processes at low energies which involve hydrogen ion, atoms, and molecules, Atomic and Plasma-material Interaction Data for Fusion , 135 (2001).

[25] A. Rousseau, G. Cartry, and X. Duten, Surface recombination of hydrogen atoms studied by a pulsed plasma excitation technique, J. Appl. Phys. **89**, 2074 (2001).

[26] A. Rousseau, A. Granier, G. Gousset, and P. Leprince, Microwave discharge in H_2: influence of h-atom density on the power balance, J. Phys. D: Appl. Phys. **27**, 1412 (1994).

[27] C. M. Samuell *et al.*, *Hydrogen plasmas and their interaction with fusion-relevant materials*, Ph.D. thesis, The Australian National University (2014).

[28] D. Lopaev and A. Smirnov, Diagnostics of heterogeneous processes with the participation of radicals by time-resolved actinometry, Plasma Phys. Rep. **30**, 882 (2004).

[29] S. Zyryanov, A. Kovalev, D. Lopaev, E. Malykhin, A. Rakhimov, T. Rakhimova, K. Koshelev, and V. Krivtsun, Loss of hydrogen atoms in H_2 plasma on the surfaces of materials used in euv lithography, Plasma Phys. Rep. **37**, 881 (2011).

[30] B. J. Wood and H. Wise, The kinetics of hydrogen atom recombination on pyrex glass and fused quartz1, The Journal of Physical Chemistry **66**, 1049 (1962).

[31] C. Samuell and C. Corr, Ion flux dependence of atomic hydrogen loss probabilities on tungsten and carbon surfaces, J. Nucl. Mater. **451**, 211 (2014).

[32] G. Cartry, L. Magne, and G. Cernogora, Atomic oxygen recombination on fused silica: experimental evidence of the surface state influence, J. Phys. D: Appl. Phys. **32**, L53 (1999).

[33] G. Cartry, X. Duten, and A. Rousseau, Atomic oxygen surface loss probability on silica in microwave plasmas studied by a pulsed induced fluorescence technique, Plasma Sources Sci.

Technol. **15**, 479 (2006).

[34] K. K. Mackay, H. T. Johnson, and J. B. Freund, Poisoning of hydrogen recombination on silica due to water adsorption, The Journal of Physical Chemistry C **121**, 16366 (2017).

[35] Y. Abe, S. Kawashima, K. Takeda, M. Sekine, and M. Hori, Dependence of surface-loss probability of hydrogen atom on pressures in very high frequency parallel-plate capacitively coupled plasma, Appl. Phys Express **3**, 106001 (2010).

[36] J. Jolly and J.-P. Booth, Atomic hydrogen densities in capacitively coupled very high-frequency plasmas in H_2: Effect of excitation frequency, J. Appl. Phys. **97**, 103305 (2005).

[37] P. Kae-Nune, J. Perrin, J. Jolly, and J. Guillon, Surface recombination probabilities of H on stainless steel, a-Si: H and oxidized silicon determined by threshold ionization mass spectrometry in H_2 rf discharges, Surf. Sci. **360**, L495 (1996).

[38] S. Takashima, M. Hori, T. Goto, A. Kono, and K. Yoneda, Absolute concentration and loss kinetics of hydrogen atom in methane and hydrogen plasmas, J. Appl. Phys. **90**, 5497 (2001).

[39] A. D. Tserepi and T. A. Miller, Two-photon absorption laser-induced fluorescence of H atoms: A probe for heterogeneous processes in hydrogen plasmas, J. Appl. Phys. **75**, 7231 (1994).

[40] M. Sode, T. Schwarz-Selinger, W. Jacob, and H. Kersten, Surface loss probability of atomic hydrogen for different electrode cover materials investigated in h2-ar low-pressure plasmas, J. Appl. Phys. **116**, 013302 (2014).

[41] M. E. Galante, *Two-Photon Absorption Laser Induced Fluorescence Measurements of Neutral Density in Helicon Plasma*, Graduate theses, dissertations, and problem reports., West Virginia University (2013).

[42] J.-S. Yoon, M.-Y. Song, J.-M. Han, S. H. Hwang, W.-S. Chang, B. Lee, and Y. Itikawa, Cross sections for electron collisions with hydrogen molecules, J. Phys. Chem. Ref. Data **37**, 913 (2008).

[43] J.-S. Yoon, Y.-W. Kim, D.-C. Kwon, M.-Y. Song, W.-S. Chang, C.-G. Kim, V. Kumar, and B. Lee, Electron-impact cross sections for deuterated hydrogen and deuterium molecules, Rep. Prog. Phys. **73**, 116401 (2010).

[44] M. C. Zammit, J. S. Savage, D. V. Fursa, and I. Bray, Electron-impact excitation of molecular hydrogen, Phys. Rev. A **95**, 022708 (2017).

[45] R. Janev, D. Post, K. Evans, and W. Langer, *Elementary processes in hydrogen-helium plasmas: cross sections and reaction rate coefficients* (Springer, 1987).

[46] D. Fursa, L. Scarlett, J. Tapley, J. Savage, M. Zammit, M. Zawadzki, R. Wright, G. Dolmat, M. Martin, L. Hargreaves, and M. Khakoo, Electron-impact dissociation of molecular hydrogen: benchmark cross sections, in *Proceedings of the 45th* EPS *Conference on Plasma Physics* (European Physical Society, 2018) p. P5.3012.

[47] L. H. Scarlett, J. K. Tapley, D. V. Fursa, M. C. Zammit, J. S. Savage, and I. Bray, Low-energy electron-impact dissociative excitation of molecular hydrogen and its isotopologues, Phys. Rev. A **96**, 062708 (2017).

[48] C. S. Trevisan and J. Tennyson, Calculated rates for the electron impact dissociation of molecular hydrogen, deuterium and tritium, Plasma Phys. Controlled Fusion **44**, 1263 (2002).

[49] R. Celiberto, R. Janev, A. Laricchiuta, M. Capitelli, J. Wadehra, and D. Atems, Cross section data for electron-impact inelastic processes of vibrationally excited molecules of hydrogen and its isotopes, At. Data Nucl. Data Tables **77**, 161 (2001).

[50] Data have been retrieved on August 22, 2019 from CCC database, www.lxcat.net.

[51] E. Krishnakumar, S. Denifl, I. Čadež, S. Markelj, and N. Mason, Dissociative electron attachment cross sections for H_2 and D_2, Phys. Rev. Lett. **106**, 243201 (2011).

[52] M. A. Lieberman and A. J. Lichtenberg, *Principles of plasma discharges and materials processing* (John Wiley & Sons, 2005).

[53] P. Chabert and N. Braithwaite, *Physics of radio-frequency plasmas* (Cambridge University Press, 2011).

[54] D. Rapp, T. Sharp, and D. Briglia, Large isotope effect in the formation of H− orH− by electron impact on H_2, HD, andD_2, Phys. Rev. Lett. **14**, 533 (1965).

[55] J. Horáček, M. Čížek, K. Houfek, P. Kolorenč, and W. Domcke, Dissociative electron attachment and vibrational excitation of H_2 by low-energy electrons: Calculations based on an improved non-local resonance model, Phys. Rev. A **70**, 052712 (2004).

[56] M. Bacal and M. Wada, Negative ion source operation with deuterium, Plasma Sources Sci. Technol. **29**, 033001 (2020).

[57] J. Wadehra and J. Bardsley, Vibrational-and rotational-state dependence of dissociative attachment in e-H_2 collisions, Phys. Rev. Lett. **41**, 1795 (1978).

[58] R. K. Janev, D. Reiter, and U. Samm, *Collision processes in low-temperature hydrogen plasmas* (Forschungszentrum Jülich, Zentralbibliothek, 2003).

[59] A. Morillo-Candas, T. Silva, B. Klarenaar, M. Grofulović, V. Guerra, and O. Guaitella, Elec-

tron impact dissociation of CO_2, Plasma Sources Sci. Technol. **29**, 01LT01 (2020).

[60] X. Duan and H. Lange, Effect of laser property fluctuations over multipulses on H atom measurement by two-photon absorption laser-induced fluorescence, J. Phys. B: At., Mol. Opt. Phys. **37**, 427 (2003).

[61] J. Bokor, R. Freeman, J. White, and R. Storz, Two-photon excitation of the n= 3 level in H and D atoms, Phys. Rev. A **24**, 612 (1981).

[62] M. Galante, R. Magee, and E. Scime, Two photon absorption laser induced fluorescence measurements of neutral density in a helicon plasma, Phys. Plasmas **21**, 055704 (2014).